Molybdenum Sulfide – Reduced Graphene Oxide *p-n* Heterojunction Nanosheets with Anchored Oxygen Generating Manganese Dioxide Nanoparticles for Enhanced Photodynamic Therapy

Sutanu Kapri and Sayan Bhattacharyya*

Department of Chemical Sciences, and Centre for Advanced Functional Materials, Indian Institute of Science Education and Research (IISER) Kolkata, Mohanpur - 741246, India

*Email for Correspondence: sayanb@iiserkol.ac.in

S1. Experimental Section

Materials

Graphite flakes (99.9% metal basis, Alfa Aesar), sodium molybdate dihydrate (Na_2MoO_4, $2H_2O$, 98%, Merck, India), thiourea (≥99%, Merck, India), manganese (II) choloride tetrahydrate (MnO_2, 99%, Merck, India), alfa lipoic acid (≥99%, Sigma Aldrich), poly (ethylene glycol) methyl ether (M_w = 2000), Sigma Aldrich), sodium hydroxide (NaOH, ≥97%, Merck, India), sodium chloride (NaCl, 99.5%, Merck, India), hydrogen peroxide (H_2O_2, 30%, Merck), silicon wafer (Sigma Aldrich), Ethanol, acetonitrile (CH_3CN), and acetone were used as received (Merck, India). Dialysis membrane (MWCO 3500, Fischer Scientific), 1,3-Diphenylisobenzofuran (DPBF, 97%, Sigma Aldrich), deuterium oxide (D_2O, 99.9%, cambridge Isotope Laboratories, Inc.), 1-Methyl-2-pyrrolidone (NMP, 99%), polyvinylidene fluoride (PVDF) powder were purchased from Sigma Aldrich. F:SnO_2 (FTO)-coated glass (TCO 22-7). fluorescein diacetate (FDA, Sigma Aldrich), propidium iodide (PI, ≥94%, HPLC, Sigma Aldrich), potassium bromide (KBr, FTIR grade), Trypsin/EDTA solution (Gibco), dulbecco's modified eagle media (DMEM, Gibco), fetal bovine serum (FBS, Hyclone, Thermo Scientific), 3-(4,5-dimethylthiazol-2-yl)-2,5-diphenyltetrazolium bromide (MTT, USB Corporation), dimethyl sulphoxide (DMSO, 99.9% molecular biology grade, Sigma Aldrich), 2′,7′-Dichlorodihydrofluorescein diacetate (DCFH-DA, >97%, Sigma Aldrich), fetal bovine serum (FBS, Hyclone, Thermo Scientific), Alexa Fluor® 488 Annexin V/Dead Cell Apoptosis Kit (Thermo Fisher Scientific), were used without further purification.

Instrumentation

Nitrogen doping of the heterojunction nanosheets was performed in a Carbolite wire-wound tube furnace-single zone, model MTF 12/38/400. UV-vis absorption spectra were recorded on a JASCO V-670 spectrophotometer. Fluorescence spectra were performed on a Horiba Scientific Fluoromax-4 spectrofluorometer using a Xe lamp as the excitation source with a wavelength of 309 nm. X-ray diffraction (XRD) were carried out with a Rigaku (mini flex II, Japan) powder X-ray diffractometer having Cu Kα = 1.54059 Å radiation. Field emission scanning electron microscope (FESEM) images were obtained using Carl Zeiss SUPRA 55VP FESEM. Energy dispersive analysis of X-rays (EDAX) studies were carried out with the Oxford Instruments X-Max with INCA software coupled to the FESEM. For

transmission electron microscopy (TEM) imaging, ethanolic dispersions of the as-prepared samples were ultrasonicated to obtain a stable dispersion of the particles. One drop of this solution was drop casted onto the carbon coated Cu-based grid (Ted Pella, Inc., 300 mesh Cu) and were recorded in JEOL, JEM 2100 HR model. TEM images on STEM (HAADF) mode were taken in the UHR-FEG-TEM, DST-FIST facility of IISER Kolkata. AFM imaging was performed using NT-MDT NTEGRA instrument from NT-MDT (Santa Clara, CA). The zeta potential of the NPs was measured with a Malvern Zetasizer Nano ZS dynamic light scattering (DLS) instrument. The Fourier transform infrared (FTIR) spectroscopy studies were carried out with a Perkin Elmer spectrum RX1 with KBr pellets. Raman spectra were recorded with 633 nm line of a He-Ne ion laser as the excitation source (LABRAM HR800) to analyze the nanorods and PDA coating. N_2 adsorption-desorption isotherms were performed on a Micromeritics Gemini VII surface area analyser and reported by BJH (Barrett-Joyner-Halenda) surface/volume mesopore analysis. Samples were degassed at 100°C under N_2 atmosphere for 6 h. The specific surface area was determined according to the Brunauer-Emmett–Teller (BET) method. O_2 concentration was measured by a dissolved oxygen meter (ProODO, YSI). Fluorescence microscopy images and live dead cell experiments were performed by Olympus IX83 microscope with Hamamatsu ORCA-Flash 4.0 camera. Flow cytometry experiments were carried out in Fluorescence-activated cell sorting (FACS) instrument (BD FACSVerse^{TM}).

Material Synthesis

Synthesis of GO

GO was prepared by modified Hummer's method.[S1] Briefly, 0.75 g graphite flakes was manually powdered with 25 g NaCl, dissolved in water and filtered to remove NaCl. The dried graphitic flakes were vigorously stirred in 20 ml H_2SO_4 for 12 h before adding 3.5 g $KMnO_4$ while keeping the temperature at 20^{o}C. The solution was then stirred at 70^{o}C for 60 min, the temperature increased to 90^{o}C and stirred for 90 min. 30 ml H_2O was added into the reaction vessel and temperature was again increased to 110 ^{o}C under stirring for 30 min. After cooling, 60 ml water and 5 ml 30% H_2O_2 were added drop wise under vigorous stirring. For purification, the obtained solution was ultrasonicated for 10 min and repeatedly washed with 5% HCl, water and ethanol until the pH of the solution reached ~7. Finally the products were dried in hot air oven at 60 ^{o}C overnight and collected for further use.

Synthesis of MoS_2 and MoS_2/rGO nanosheets

Layered MoS_2/rGO was synthesized by routine hydrothermal technique. 0.25 mmol $Na_2MoO_4.2H_2O$ and 0.7 mmol thiourea were dissolved in 30 mL distilled water, and then 50 mg of as synthesized GO was added and ultrasonicated for 10 min to form a homogeneous solution. The solution was heated inside a 50 mL Teflon-lined autoclave at 180 ^oC for 16 h. Thereafter the solution was ultrasonicated for 5 min and subsequently washed with water and ethanol multiple times by centrifugation at 13000 rpm for 20 min. Finally MoS_2/rGO nanosheets were oven dried at 60 ^oC overnight. For the preparation of bare MoS_2, similar hydrothermal method was used without adding GO into the solution.

Synthesis of p-MoS_2/n-rGO heterojunction nanosheets

To obtain *p*-MoS_2/*n*-rGO heterojunction nanosheets, the as-prepared MoS_2/rGO nanosheets were heated at 500 ^oC for 45 min with a ramp rate of 3 ^oC/min under NH_3 flow.[S2] After completion of the reaction, N-doped MoS_2/rGO nanosheets were collected and dispersed in water : ethanol (1:1 v/v) for 5 min ultrasonication. Finally the product was washed with ethanol and water thrice and dried in an oven for further use.

Synthesis of p-MoS_2/n-rGO-MnO_2 heterojunction nanosheets

For the preparation of MnO_2 NP decorated *p*-MoS_2/*n*-rGO, 100 mg *p*-MoS_2/*n*-rGO nanosheets were mixed with 10 mg $MnCl_2.4H_2O$ in 50 ml distilled water and ultrasonicated for 20 min to form a homogeneous mixture. 5 ml of $KMnO_4$ solution (1 mg/ml) was added drop by drop to the reaction mixture in a round bottom flask under vigorous stirring for 10 h. Thereafter the solution was washed multiple times with ethanol and water. Finally *p*-MoS_2/*n*-rGO-MnO_2 was collected and dried under vacuum for further use.

Synthesis of LA-PEG

LA-PEG was synthesized by an earlier reported method with slight modifications.[S3] Briefly, 1g poly (ethylene glycol) methyl ether (M_w = 2000) and 100 mg of α-lipoic acid was degassed under stirring at 50 ^oC in N_2 atmosphere. 20 mL toluene dispersion of 12 mg $HfCl_4.2THF$ was injected into the reaction vessel and refluxed at 130 ^oC for 24 h. Toluene was removed by rotary evaporator under reduced pressure and the crude product was

solubilized in dichloromethane and reprecipitated into diethyl ether thrice to obtain LA-PEG which was dried under vacuum for further use.

Synthesis of MoS_2/rGO-PEG, p-MoS_2/n-rGO-PEG and p-MoS_2/n-rGO-MnO_2-PEG

In order to attach LA-PEG onto the surface of the nanosheets, 20 mg of LA-PEG was dispersed in 5 ml nanosheet solution (0.25 mg/ml) under stirring for 10 min and subsequently bath sonicated for 20 min, stirred for another 12 h and centrifuged at 13000 rpm for 20 min. The PEGyalated nanosheets were washed with ethanol and water to remove excess LA-PEG and dried under high vacuum. These nanosheets were resuspended in PBS solution and stored at 40 °C for further use.

Electrode fabrication for electrochemical impedance spectral (EIS) measurements

A CHI 6005E electrochemical workstation was utilized to evaluate the Mott-Schottky plots using the standard three-electrode electrochemical cell setup with Ag/AgCl and Pt-rod as reference and counter electrode, respectively. A paste of the nanosheets was prepared by stirring overnight a mixture of 100 mg of the nanosheets, 10 mg PVDF and 300 μL NMP. The paste was doctor bladed on pre-cleaned FTO with an active area of 1 cm^2. Finally, the samples were dried in a hot air oven at 80°C for 2 h.

Extracellular O_2 detection by *p*-MoS_2/*n*-rGO-MnO_2-PEG nanosheets

p-MoS_2/*n*-rGO-MnO_2-PEG nanosheets in a series of different concentrations were dispersed in water containing 1×10^{-3} M H_2O_2 and the oxygen levels were monitored over time by dissolved oxygen meter. The O_2 evolution capability of bare H_2O_2 and *p*-MoS_2/*n*-rGO-MnO_2-PEG dispersion without H_2O_2 was measured in N_2 saturated solution.

Singlet Oxygen Generation by Nanosheets

Generation of $^1O_2$ phosphorescence

For $^1O_2$ emission experiments, firstly, *p*-MoS_2/*n*-rGO-PEG, *p*-MoS_2/*n*-rGO-MnO_2-PEG and standard photosensitizer rose Bengal (RB) each dispersed in 15:1 (v/v) CH_3CN:D_2O solution were taken in a quartz cuvette and placed in the fluorescence spectrometer with a 980 nm excitation laser and NIR detector. The $^1O_2$ quantum yield of the nanosheets was calculated using the formula:

$\Phi_{NS} = \Phi_{RB} (I_{NS}/ I_{RB})$ (S1)

where I_{NS} and I_{RB} represent the PL peak areas of $^1O_2$ produced by the nanosheet and RB, respectively.[S4]

Extracellular and Intracellular ROS Detection

DPBF was used to detect extracellular $^1O_2$ nanosheets in the presence or absence of H_2O_2 and singlet oxygen scavenger NaN_3 under 980 laser irradiation (0.4 W/cm^2) for 5 min. 50 µl ethanolic solution of DPBF (1 mg/ml) was added into the nanosheets solution under stirring and irradiated with NIR laser for different time periods. Then the solution was collected and UV-vis spectra were performed and the DPBF absorbance was monitored at 415 nm. The decrease in absorbance was due to the degradation of DPBF by $^1O_2$ which was generated by the nanosheets in presence of NIR laser.

For intracellular ROS detection, HeLa cells were incubated in 24-well plate with the nanosheets (60 µg/ml) and 5% CO_2 at 37 ^{o}C for 12 h. Thereafter the cells were washed with PBS thrice and serum free medium containing DCFH-DA (10 µM) was added into the well plate and incubated for another 30 min. The cells were then washed with PBS thrice to remove excess DCFH-DA. Finally the incubated cells were irradiated with 980 nm NIR laser (0.4 W/cm^2) for 5 min and fluorescence images were acquired by TIRF microscope with 485 nm excitation and emission at 525 nm.

Intracellular Toxicity of Nanosheets

To evaluate the cell viability of nanosheets, MTT assay was conducted against HeLa and HEK 293 cells. Firstly, cells were seeded and grown into 24-well plate at 1 × 10^5 cells per 1 mL of 10% FBS containing DMEM media (MEM for HEK 293 cell) at 37 ^{o}C, 5% CO_2 in a humidified incubator. When the cells were confluent to 65-80 %, they were washed with PBS and the cell media containing different concentrations of nanosheets (i.e., 25, 50, 100, 200 µg/ml) were added and incubated for 24 h. After 24 h, each well was washed with PBS buffer (pH 7.4) thrice to remove the non-specifically bound nanosheets. 100 µl of freshly prepared MTT solution (5 mg/mL) was added to each well and incubated at 37 ^{o}C for next 4 h. Finally the cell culture media was discarded and 500 µl of DMSO was added to each well and subsequently the 24-well plates were shaken gently at room temperature. At least three parallel samples were performed in each group and all the sets were tested with triplicates.

The relative cell viability of the cells was measured by the absorbance at 570 nm. The cell viability (%) was calculated according to the following equation (S2):[S5]

Cell viability (%) = [{OD@570 nm (sample)}/{OD@570 nm (Control)}]*100 (S2)

where OD is the optical density.

To investigate the *in vitro* PDT effect of the nanosheets, HeLa cells were grown into 96-well plate and incubated for 24 h in a 5% CO_2 incubator at 37 °C. After 24 h, cell media containing the nanosheets (MoS_2/rGO-PEG, *p*-MoS_2/*n*-rGO-PEG and *p*-MoS_2/*n*-rGO-MnO_2-PEG) were added into each well and incubated for 12 h. To remove excess nanosheets, the cells were carefully washed with PBS thrice and replaced with fresh cultured media. Thereafter the cells were subjected to irradiation with 980 nm laser for 5 min (0.4 W/cm^2), and cultured again for another 24 h. Finally, the aforementioned MTT assay was conducted to evaluate the relative cell viability of the nanosheets while control experiments did not include any nanosheet.

In order to intuitively observe the intracellular PDT therapeutic effect of nanosheets, the live and dead cells were co-stained with fluorescein diacetate (FDA) and PI under irradiation with 980 nm NIR laser. HeLa cells were seeded into 35 mm petri dishes (2 ml, 3 × 10^4 cells per well) and incubated for 24 h at 37 ^{o}C. After treatment with cell culture media containing the nanosheets (60 μg/mL) for 4 h, the cells were irradiated with NIR laser for 5 min and the culture was continued for another 12 h. Thereafter, the cells were carefully washed with PBS twice. After staining with a mixture of FDA/PI in FBS free media for 15 min, followed by washing with PBS twice, the fluorescence images were recorded using epifluorescence microscope.

Photothermal Performance of *p*-MoS_2/*n*-rGO-MnO_2-PEG, MoS_2/rGO-PEG, *p*-MoS_2/*n*-rGO-PEG

Firstly, different concentrations (20, 40, 60 and 80 μg/mL) of *p*-MoS_2/*n*-rGO-MnO_2-PEG were dispersed in PBS solution and 1 mL of the dispersions was placed inside a quartz cuvette and irradiated with 980 nm laser at a power density of 0.4 W/cm^2. The 60 μg/mL sample was irradiated with various power densities (0.2, 0.4, 0.8 and 1.6 W/cm^2) of the laser. To check the photothermal performance of MoS_2/rGO-PEG and *p*-MoS_2/*n*-rGO-PEG

nanosheets, 60 μg/mL dispersion of nanosheets were placed in the quartz cuvette and photothermal performance was evaluated by the aforementioned procedure.

Flow Cytometry Assay

To confirm the ROS generation by the nanosheets, flow cytometry was carried out to measure ROS level inside HeLa cells. Cells were seeded into six well plates at a density of 1 × 10^6 cells per well and incubated at 37 °C in cell culture media. The cells were then allowed to adhere on the well for 24 h. Afterwards, this media was removed and replaced with fresh media containing the nanosheets and incubated for 12 h. Then the treated cells were washed with PBS twice and further incubated with 10 μM of the fluorescent probe DCFH-DA for 20 min and replaced with fresh cultured media. These media were irradiated with 980 nm laser (0.4 W/cm^2) for 5 min followed by PBS washing of non-specifically bound DCFH-DA twice. Thereafter cells were harvested with trypsin–EDTA and incubated at 37 °C until the cells were detached from the well. 2 mL media was added into the trypsinized cell suspensions and centrifuged at 1000 rpm for 5 min followed by decantation of the supernatant. The cell pellet was resuspended in 500 μL ice cold PBS. Finally, the resultant cell suspensions were taken in Falcon™ tubes and analyzed by flow cytometry experiments using FL1-H channel (excitation 488 nm and emission 530 nm) in a flow cytometer. Mean fluorescent signals were taken for 10000 cells.

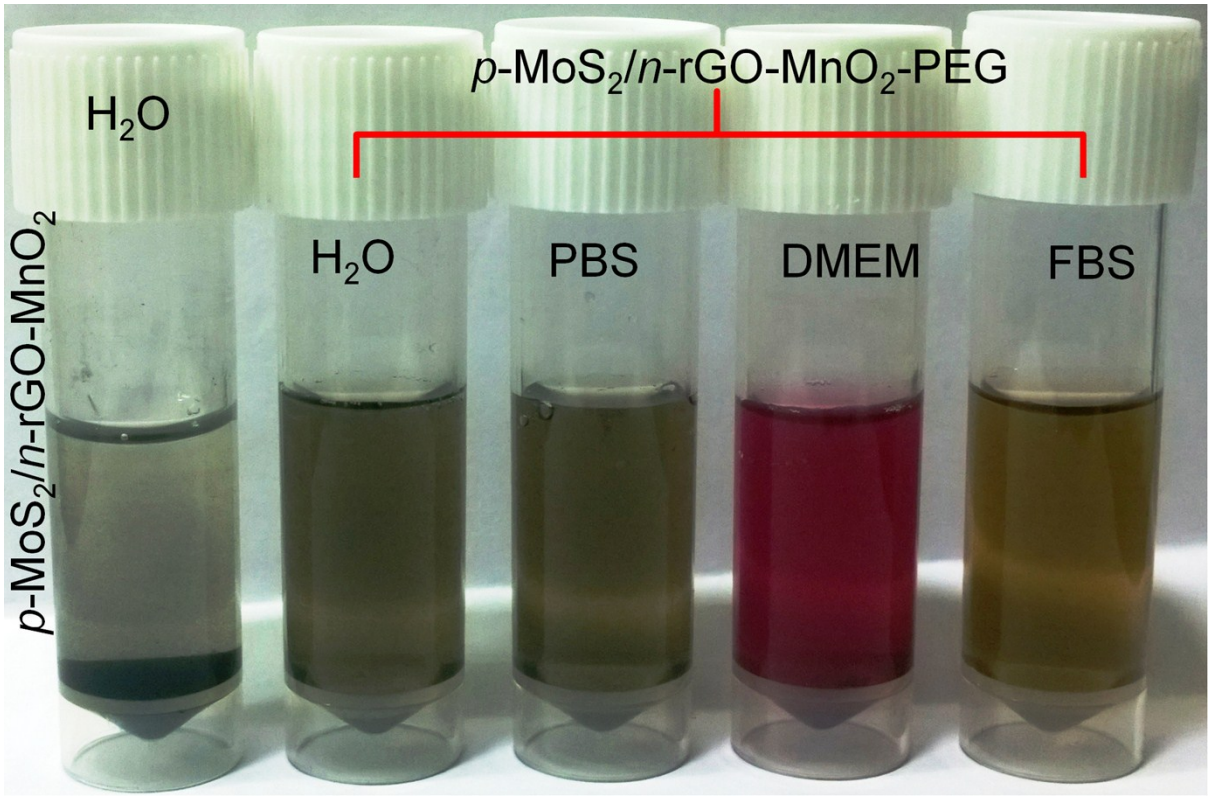

Figure S1: Digital photographs of *p*-MoS_2/*n*-rGO-MnO_2 dispersions in water and *p*-MoS_2/*n*-rGO-MnO_2-PEG dispersions in water, PBS, DMEM and FBS media, respectively.

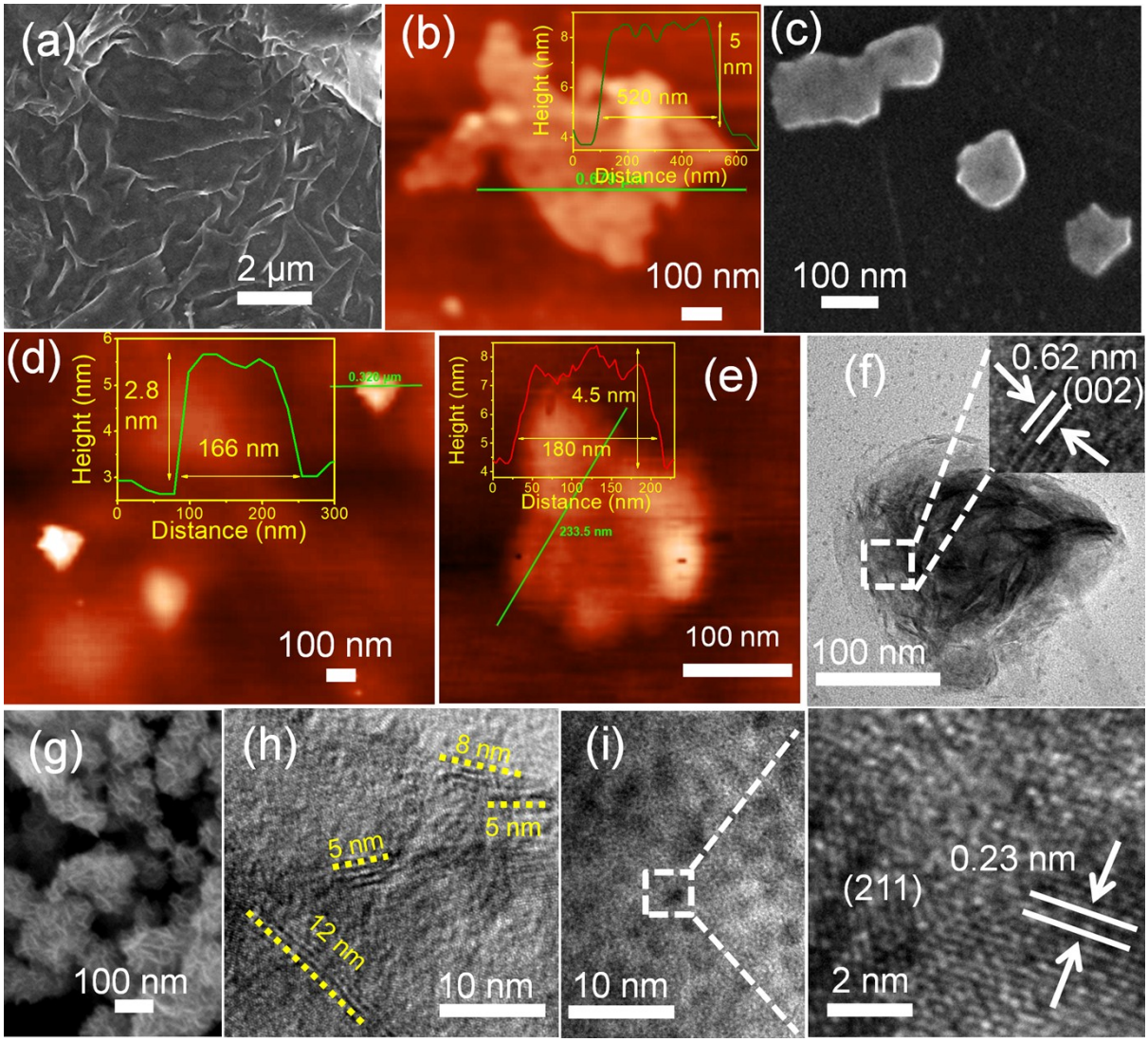

Figure S2: (a) FESEM and (b) AFM images of as synthesized GO. (c) FESEM and (d) AFM images of as exfoliated GO. (e) AFM image of *p*-MoS_2/*n*-rGO-PEG nanosheets. (f) TEM image of MoS_2/rGO-PEG nanosheets. Inset shows the corresponding lattice fringes. (g) FESEM image of bare MoS_2. (h) TEM image of *p*-MoS_2/*n*-rGO-PEG nanosheets with strip of MoS_2 nanoplates. (i) Low and high resolution TEM images of bare MnO_2 NPs. Low and high resolution TEM images of bare MnO_2 NPs.

Table S1. Elemental compositions of the nanosheets obtained from FESEM-EDS results.

Sample	**C (wt%)**	**O (wt%)**	**N (wt%)**	**Mo (wt%)**	**S (wt%)**	**Mn (wt%)**
MoS_2/rGO-PEG	29.8	25.3	2.3	25.5	17.1	-
p-MoS_2/*n*-rGO-PEG	28.1	19.1	9.1	26.3	17.4	-
p-MoS_2/*n*-rGO-MnO_2-PEG	26.3	19.9	8.7	25.1	16.4	3.6

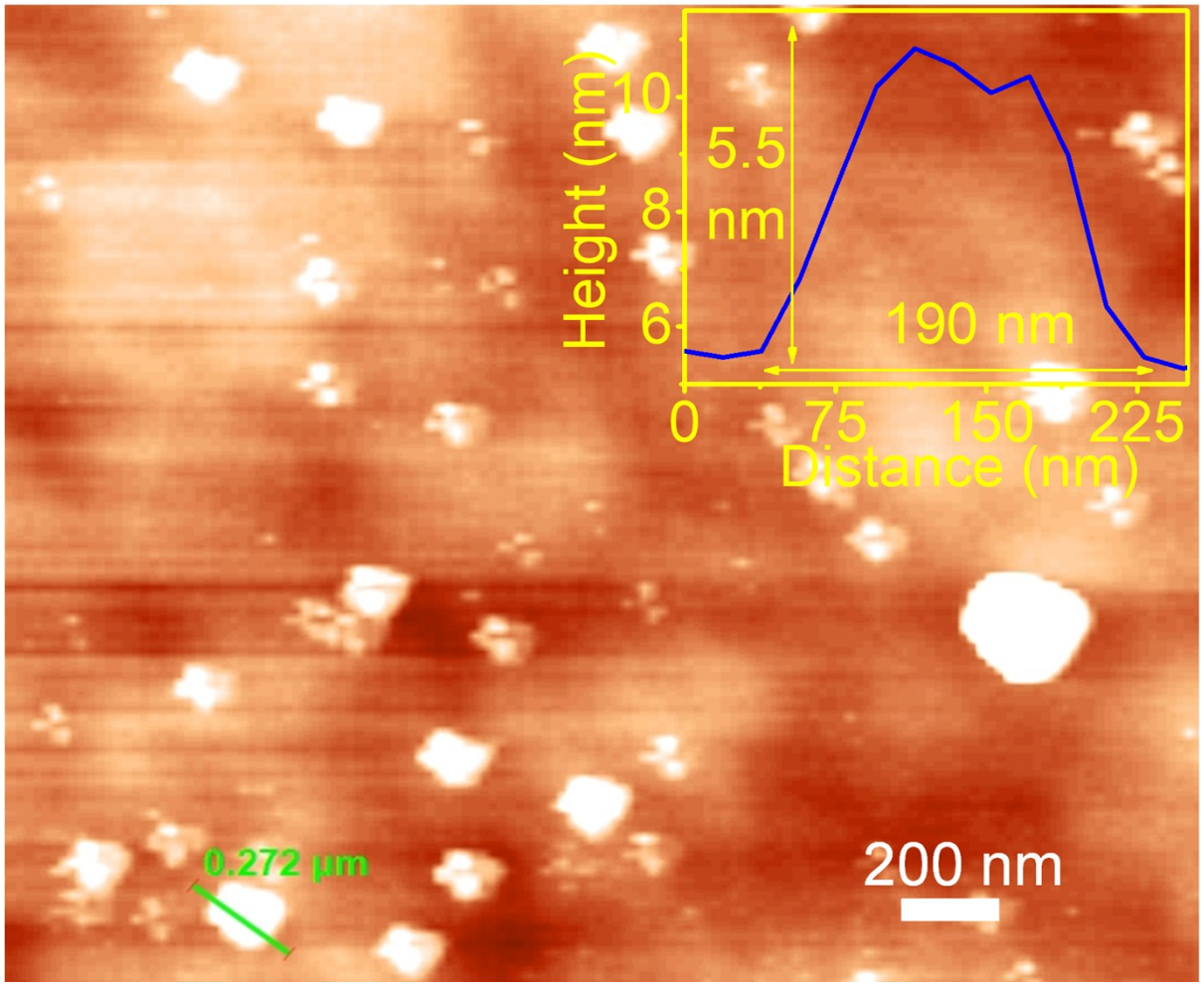

Figure S3: AFM image of *p*-MoS_2/*n*-rGO-MnO_2-PEG nanosheets. Inset shows the height profile of a selected nanosheet.

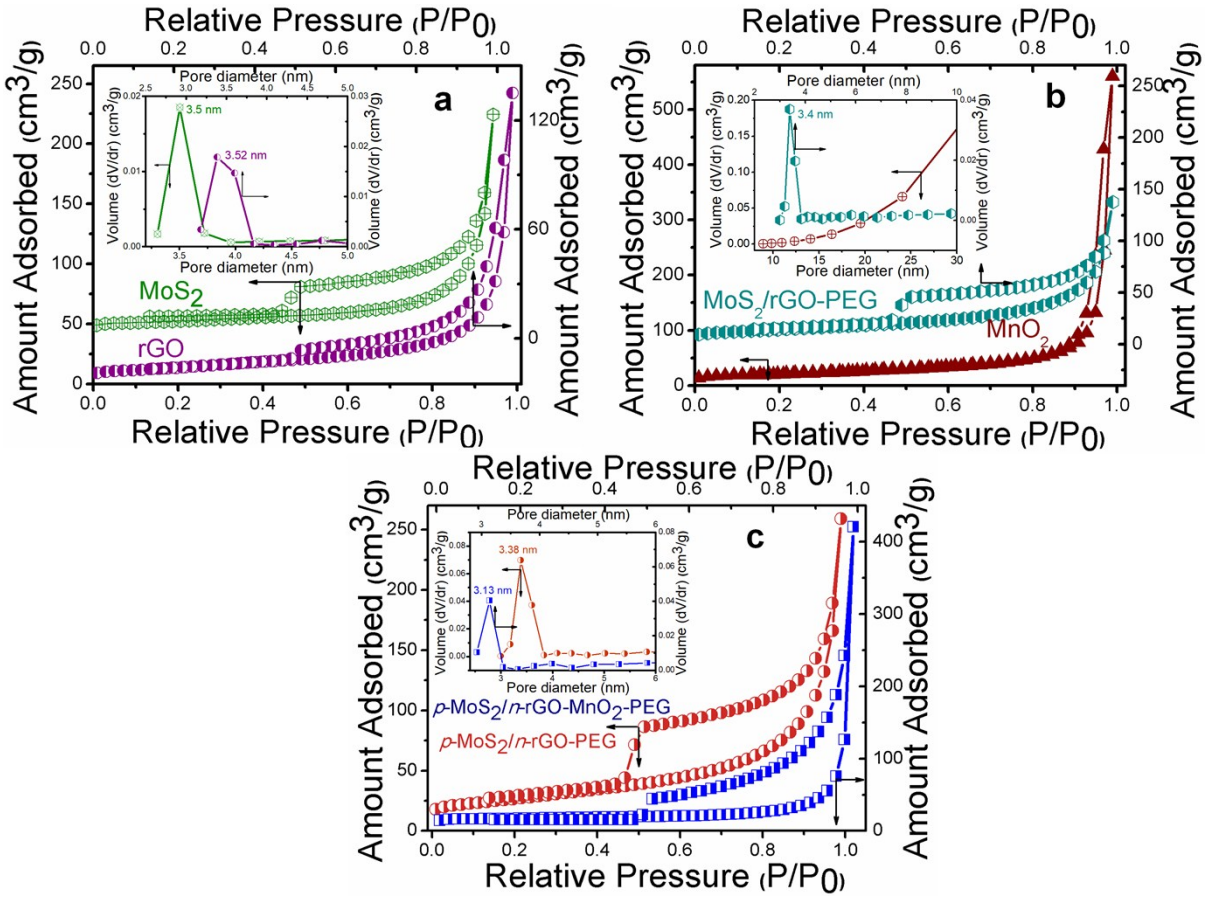

Figure S4: N_2 sorption isotherms and pore diameter distributions (inset) of (a) MoS_2 and rGO, (b) MoS_2/rGO-PEG and MnO_2, and (c) *p*-MoS_2/*n*-rGO-MnO_2-PEG and *p*-MoS_2/*n*-rGO-PEG.

The specific surface area and corresponding pore size distribution of *p*-MoS_2/*n*-rGO-MnO_2-PEG, *p*-MoS_2/*n*-rGO-PEG, MoS_2/rGO-PEG, rGO, solitary MoS_2 and bare MnO_2 were analyzed in nitrogen at 77 K and the parameters are listed in Table S2. All samples except MnO_2, display a Type IV isotherm with H3 hysteresis loop and corresponding pore size distribution ranges from 3-3.6 nm suggesting mesoporous nature. Hysteresis loop was observed in the region of relative pressure (P/P_0) = 0.45-0.95, indicating capillary condensation occurring inside mesoporous cavity. Bare MnO_2 NPs show a Type IV isotherm with H4 hysteresis loop. The high surface area and mesoporous properties of these samples open up large number of active catalytic sites which enhance the photocatalytic performance.

Table S2: Abbreviation of the samples and results from N_2 sorption measurements. SA: BET specific surface area; V: total pore volume; D: pore diameter.

Abbreviation	Sample	SA ($m^2\ g^{-1}$)	V ($cm^3\ g^{-1}$)	D (nm)
rGO	Reduced graphene oxide	31.5 ± 4	0.19	3.5
MoS_2	Molybdenum disulphide	49 ± 2	0.37	3.5
MnO_2	Manganese dioxide	74 ± 2	0.86	---
MoS_2/rGO-PEG	PEGylated MoS_2 nanoplates grown on rGO	94 ± 4	0.4	3.4
p-MoS_2/*n*-rGO-PEG	PEGylated nitrogen-doped MoS_2/rGO-PEG nanosheets	106 ± 3	0.52	3.4
p-MoS_2/*n*-rGO-MnO_2-PEG	PEGylated MnO_2 decorated *p*-MoS_2/*n*-rGO-PEG nanosheets	55 ± 2	0.65	3.1

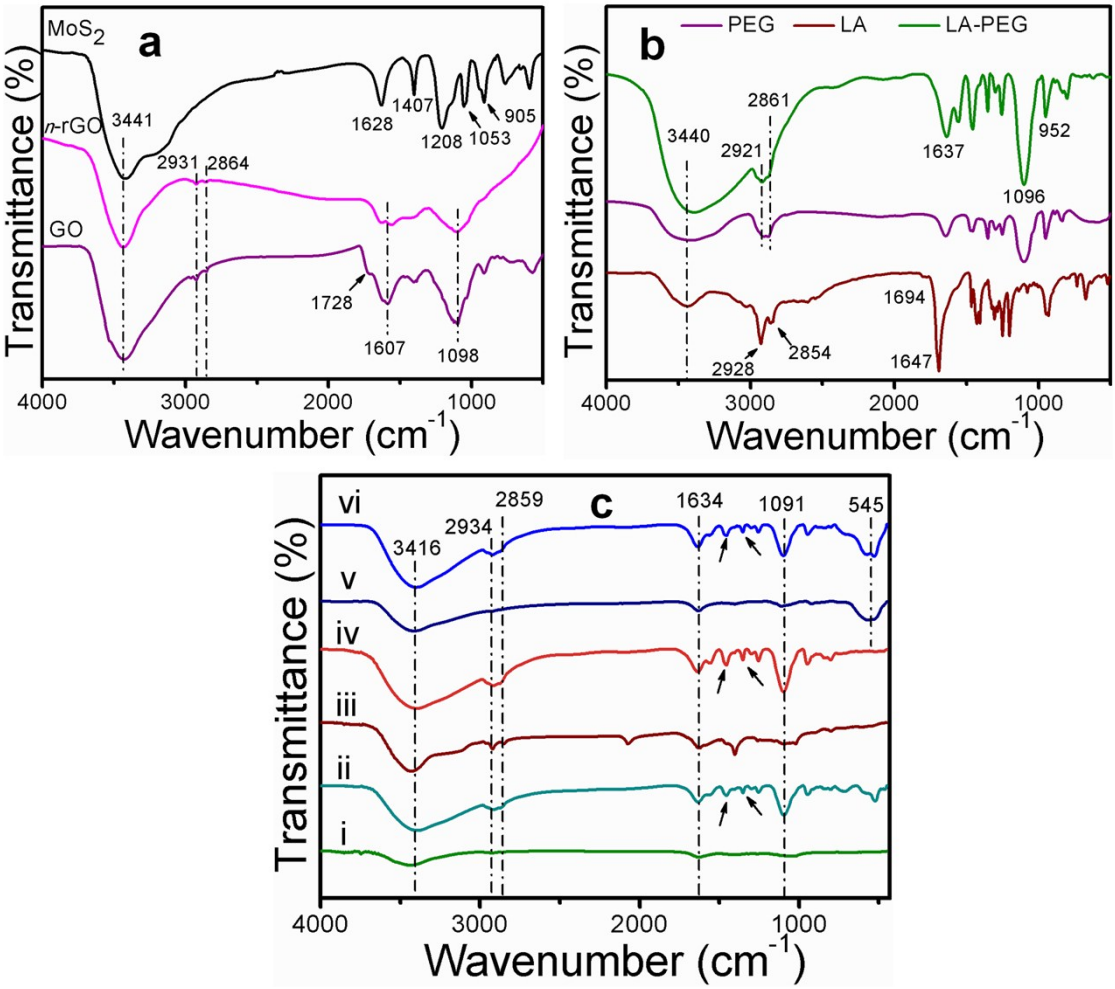

Figure S5: FTIR spectra of (a) GO, *n*-rGO and bare MoS_2, (b) PEG, LA and LA-PEG, and (c) (i) MoS_2/rGO, (ii) MoS_2/rGO-PEG, (iii) *p*-MoS_2/*n*-rGO, (iv) *p*-MoS_2/*n*-rGO-PEG, (v) *p*-MoS_2/*n*-rGO-MnO_2, (vi) *p*-MoS_2/*n*-rGO- MnO_2-PEG nanosheets.

FTIR spectroscopy was used to understand the changes of the surface chemistry of *n*-rGO nanosheets during the course of MoS_2, MnO_2 and LA-PEG immobilization. GO shows the band at 3441 cm^{-1} due to -OH vibration in graphitic plane from intra- and intermolecular hydrogen bonds between hydroxyl and carboxylic groups. The two bands at 2934 and 2864 cm^{-1} are due to the -CH stretching vibration of methylene group.[S5] Additional vibration bands at 1728, 1607 and 1098 cm^{-1} belong to carbonyl group (-C=O), C=C (skeletal vibration of graphitic domains), and C-O-C stretching vibration, respectively.[S5,S6] Similar stretching vibrations with slightly weakened bands are observed for rGO. Bare MoS_2 shows the bands at 1628, 1407, 1208, 1053 and 907 cm^{-1}. As compared to bare LA, the functionalized LA-PEG shows new vibrational bands from 1650 to 900 cm^{-1} corresponding to the characteristic vibration of PEG backbone. Those at 2928 and 2854 cm^{-1} are due to the presence of –CH stretching vibration of methylene group of both LA and PEG, respectively.[S7] These results validate the successful introduction of LA-PEG onto MoS_2/rGO, *p*-MoS_2/*n*-rGO and *p*-MoS_2/*n*-rGO-MnO_2 nanosheets. When LA-PEG is grafted onto these nanosheets new sharp bands appear at 1450, 1345 and 1249 cm^{-1}. For MoS_2/*n*-rGO-MnO_2-PEG, a broad band at 545 cm^{-1} is ascribed to Mn-O vibration in MnO_2,[S8] suggesting successful decoration of MnO_2 NPs.

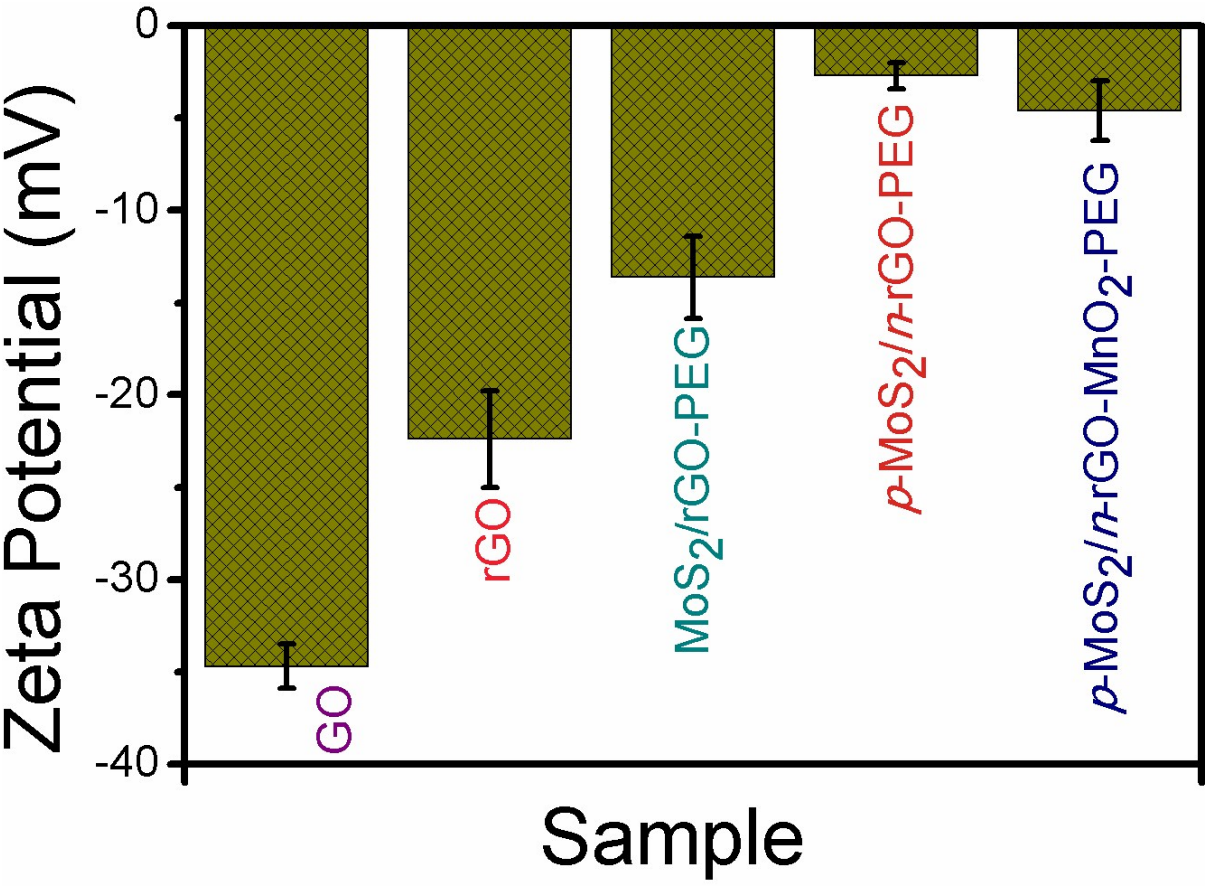

Figure S6: Zeta potential of different nanosheets.

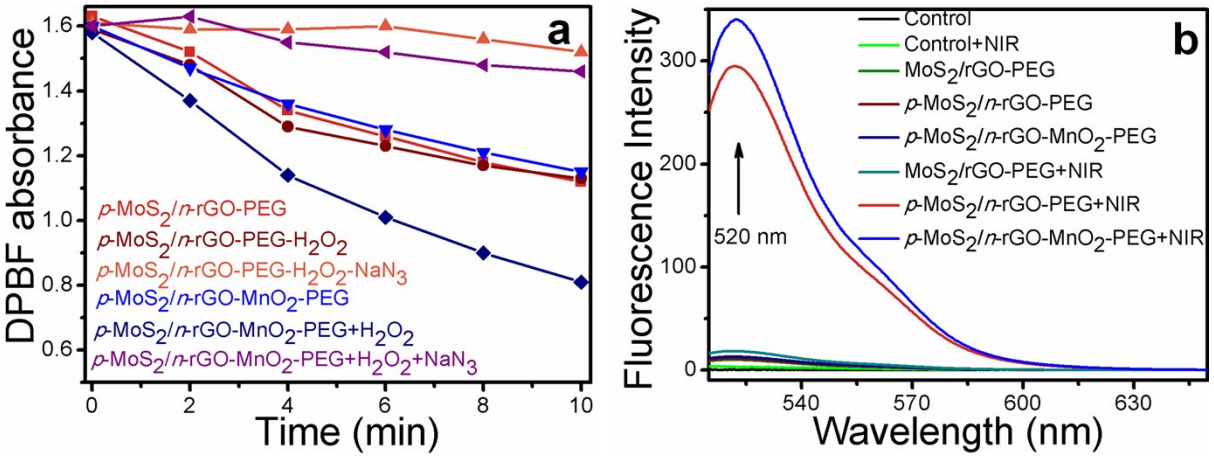

Figure S7: (a) Normalized absorbance of DPBF at a wavelength of 410 nm in the presence of nanosheets under different conditions. (b) Fluorescence spectra of DCFH incubated with MoS_2/rGO-PEG, *p*-MoS_2/*n*-rGO-PEG and *p*-MoS_2/*n*-rGO-MnO_2-PEG in the presence or absence of NIR light irradiation of 5 min.

Herein the effect of H_2O_2 and $^1O_2$ scavenger NaN_3 on $^1O_2$ generation by *p*-MoS_2/*n*-rGO-PEG and *p*-MoS_2/*n*-rGO-MnO_2-PEG nanosheets is examined by monitoring the decrease in absorbance of only DPBF in PBS or in H_2O_2 or NaN_3 solution. In the presence of H_2O_2, MnO_2 NP decorated nanosheets show high $^1O_2$ production efficacy in comparison to only heterojunction nanosheets under NIR irradiation implying *p*-MoS_2/*n*-rGO-MnO_2-PEG react with added H_2O_2 to generate significant amount of O_2 that could increase the concentration of $^1O_2$ resulting in oxidative degradation of DPBF (Figure S6a). When NaN_3 is added, the absorbance of DPBF shows no noticeable decay even after 10 min irradiation. The direct and indirect observation of $^1O_2$ phosphorescence emission and decay of DPBF absorbance, respectively, suggests *p*-MoS_2/*n*-rGO-MnO_2-PEG nanosheets can efficiently produce intracellular $^1O_2$ that kills the cancerous tissues.

Additionally, an oxidation induced fluorescent dye 2',7'-dichlorofluorescein diacetate (DCFH-DA) was used to measure ROS production by nanosheets under NIR irradiation (Figure S6b). Non fluorescent DCFH-DA is hydrolyzed by intracellular enzyme esterase and oxidized by ROS to form fluorescent 2',7'-dichlorofluorescein (DCF) via deacetylation reaction.[S9,S10] Upon NIR irradiation the fluorescence intensity of DCF at 522 nm show 19 and 16 fold increase by *p*-MoS_2/*n*-rGO-MnO_2-PEG and *p*-MoS_2/*n*-rGO-PEG as compared to MoS_2/rGO-PEG, respectively. This observation suggests that *p*-*n* heterojunction assists in producing more ROS via separation of electron and hole pair which could oxidize DCFH-DA to form fluorescent DCF. Negligible change in the fluorescence intensities is observed for only nanosheets and only NIR irradiation.

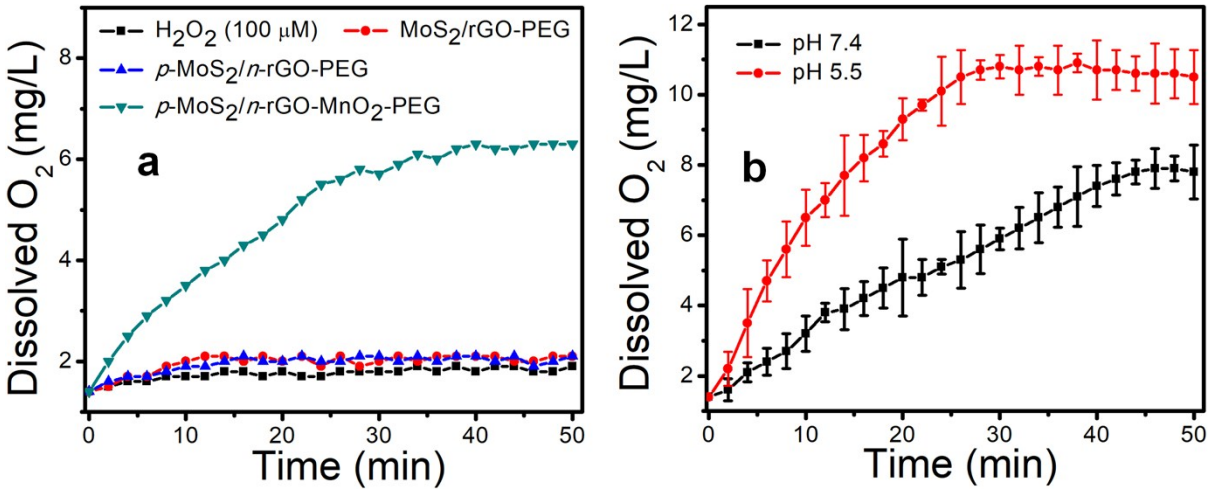

Figure S8: The changes in dissolved O_2 concentration in N_2 saturated 100 μM H_2O_2 solution with (a) MoS_2/-rGO-PEG, *p*-MoS_2/*n*-rGO-PEG and *p*-MoS_2/*n*-rGO-MnO_2-PEG nanosheets at pH 7.4, and (b) *p*-MoS_2/*n*-rGO-MnO_2-PEG at pH 5.5 and 7.4. The nanosheet concentration used is 20 μg/ml. Data is represented as mean values (±) standard deviations (n = 4).

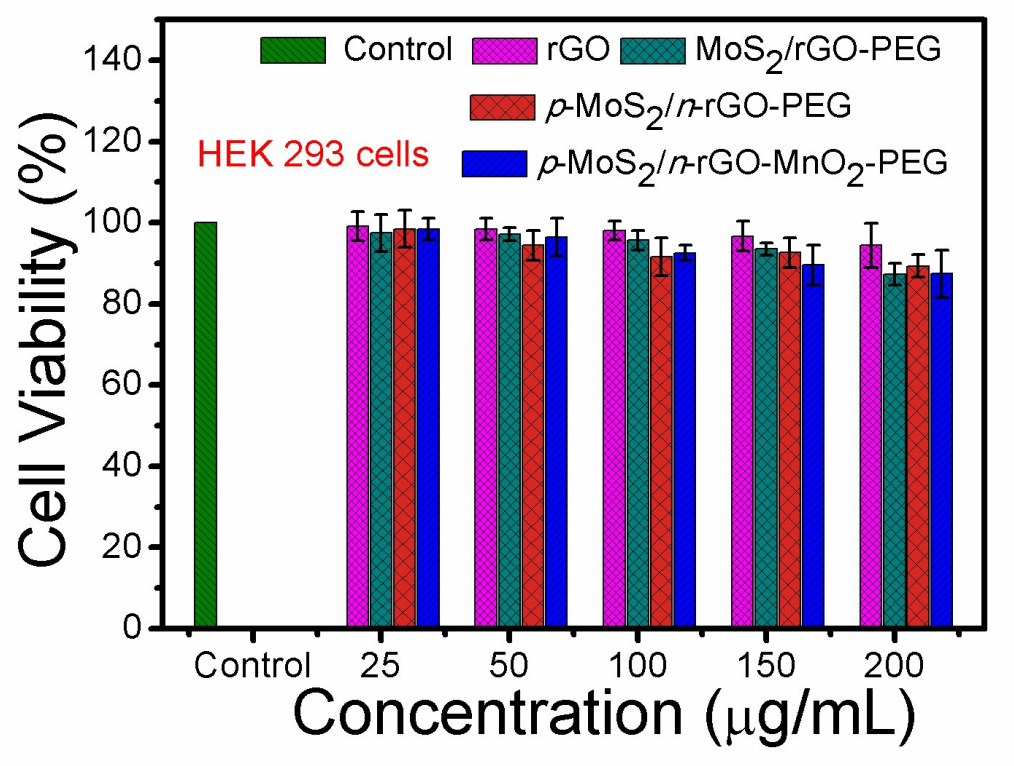

Figure S9: Cell viability of HEK 293 cells incubated with different concentrations of the nanosheets for 48h. Data is represented as mean values (±) standard deviations (n = 3).

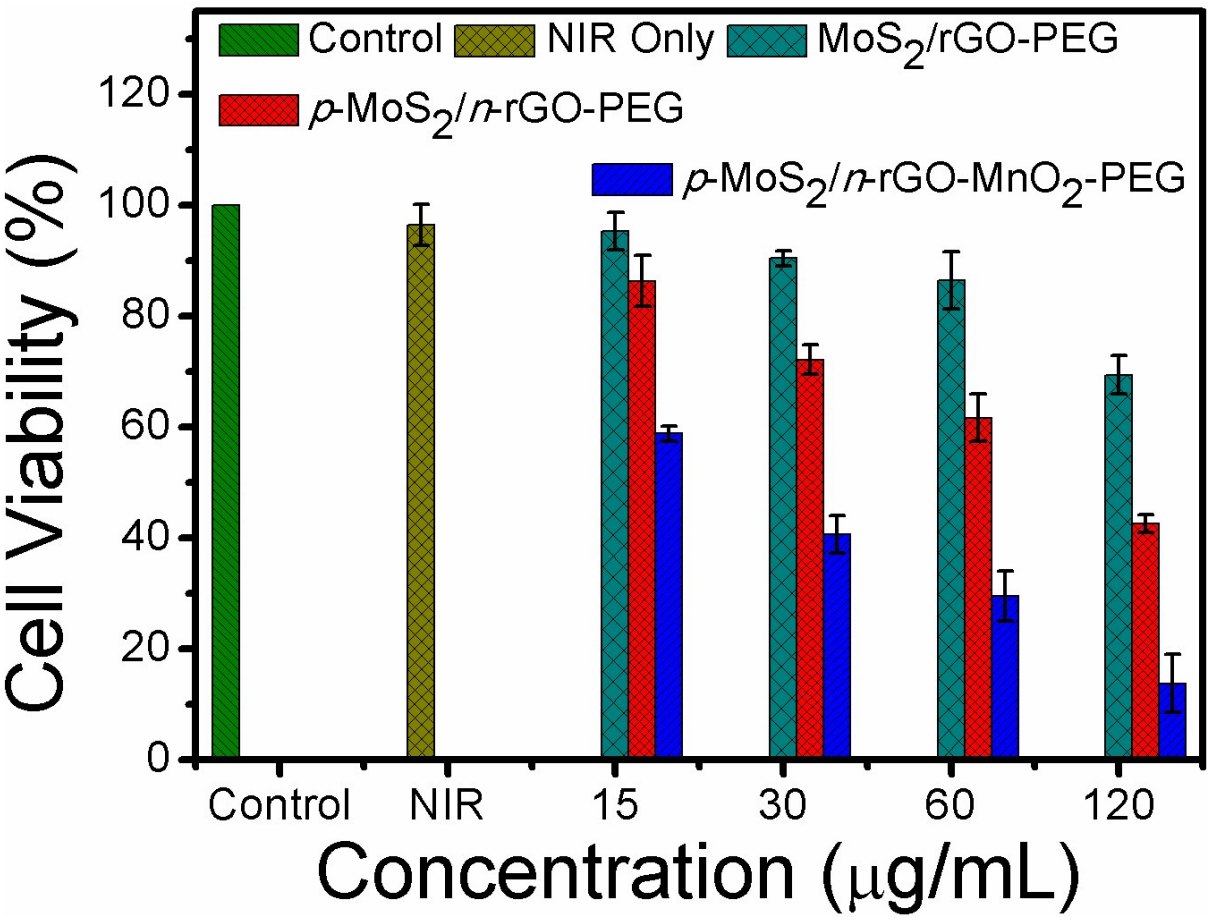

Figure S10: Cell viability of HeLa cells incubated with different concentrations of MoS_2/rGO-PEG, *p*-MoS_2/*n*-rGO-PEG and *p*-MoS_2/*n*-rGO-MnO_2-PEG in presence of NIR laser irradiation (0.4 W/cm^2) for 5 min. Data is represented as mean values (±) standard deviations (n = 3).

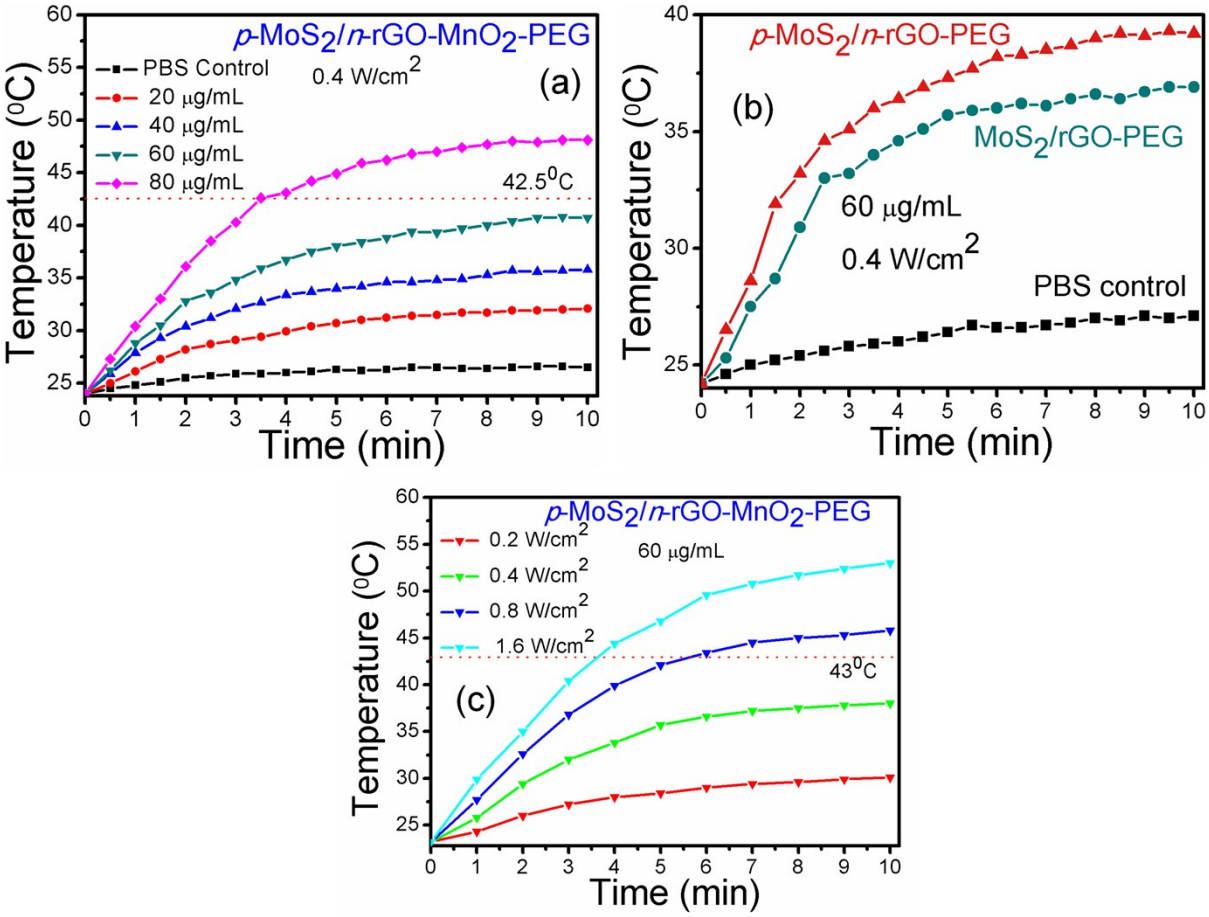

Figure S11: The temperature increment of (a) *p*-MoS_2/*n*-rGO-MnO_2-PEG at different concentrations and (b) *p*-MoS_2/*n*-rGO-PEG and MoS_2/rGO-PEG, both at a concentration of 60 μg/mL. The laser power density was fixed at 0.4 W/cm^2 for 10 min. (c) The temperature increment of *p*-MoS_2/*n*-rGO-MnO_2-PEG at a concentration of 60 μg/mL under laser irradiation with different laser power densities.

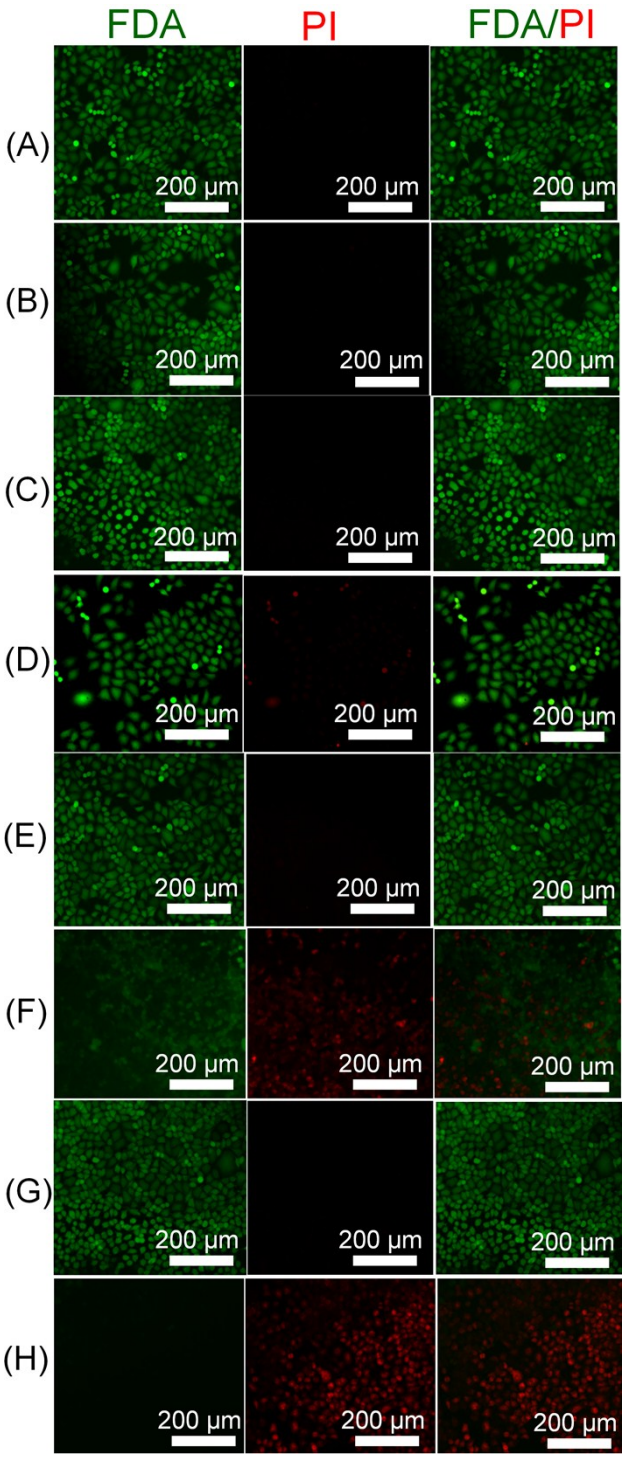

Figure S12: Epifluorescence microscopy images of fluorescein diacetate (FDA, green emission, live cells) and propidium iodide (PI, red emission, dead cells) co-stained cells in presence or absence of laser irradiation. (A) control cells, (B) only NIR, (C) only MoS_2/rGO-PEG, (D) MoS_2/rGO-PEG + NIR (0.4 W/cm^2), (E) only *p*-MoS_2/*n*-rGO-PEG, (F) *p*-MoS_2/*n*-rGO-PEG + NIR (0.4 W/cm^2), (G) only *p*-MoS_2/*n*-rGO-MnO_2-PEG, and (H) *p*-MoS_2/*n*-rGO-MnO_2-PEG + NIR (0.4 W/cm^2).

References

S1. P. Kalluru, R. Vankayala, C. S. Chiang and K. C. Hwang, *Biomaterials,* 2016, **95**, 1-10.

S2. F. Meng, J. Li, S. K. Cushing, M. Zhi and N. Wu, *J. Am. Chem. Soc.,* 2013, **135**, 10286-10289.

S3. L. Jia, D. Cui, J. Bignon, A. D. Cicco, J. Wdzieczak-Bakala, J. Liu and M. –H. Li, *Biomacromolecules,* 2014, **15**, 2206−2217.

S4. J. Ge, M. Lan, B. Zhou, W. Liu, L. Guo, H. Wang, Q. Jia, G. Niu, X. Huang, H. Zhou, X. Meng, P. Wang, C. –S. Lee, W. Zhang and X. Han, *Nat. Commun*., 2014, **5**, 4596.

S5. S. Kapri, S. Maiti and S. Bhattacharyya, *Carbon,* 2016, **100**, 223-235.

S6. D. Ghosh, G. Halder, A. Sahasrabudhe and S. Bhattacharyya, *Nanoscale,* 2016, **8**, 10632–10641.

S7. W. Feng, L. Chen, M. Qin, X. Zhou, Q. Zhang, Y. Miao, K. Qiu, Y. Zhang and C. He, *Sci. Rep.,* 2015, **5**, 17422.

S8. Z. Hua, Y. Zhao, J. Liu, J. Wanga, B. Zhang and X. Xiang, *J. Colloid Interf. Sci.,* 2016, **483**, 26-33.

S9. H. Wang, X. Yang, W. Shao, S. Chen, J. Xie, X. Zhang, J. Wang and Y. Xie, *J. Am. Chem. Soc.,* 2015, **137**, 11376– 11382.

S10. H. J. Zhu, J. C. Li, X. Y. Qi, P. Chen and K. Y. Pu, *Nano Lett.,* 2018, **18**, 586– 594.